A New Lissajous-Based Technique for Islanding Detection in Microgrid

Yadala Pavankumar, Sudipta Debnath, and Subrata Paul

***Abstract*—This study presents a novel technique for islanding detection in microgrid based on Lissajous figure of voltage and current signals. The Lissajous figure reveals distinct pattern during islanding which can segregate the islanding event from other non-islanding disturbance events such as switching transients and faults. Lissajous figures have been considered as images to capture the characterizing patterns in their shapes. The area of the Lissajous figure has been considered for successive intervals to develop an index mathematically and an appropriate adaptive threshold value of index has been formulated to detect the islanding phenomenon. The proposed technique does not require the information about the network configuration. The efficacy of the proposed technique has been established through fast islanding detection with load inside the non-detection zone (NDZ) and under the condition of complete match between the distributed sources and the load. To establish the efficacy of the proposed technique, comparative analysis has been carried out with other recent islanding detection techniques.**

***Index Terms*—Distributed generation, islanding detection, Lissajous figure, renewable energy resources.**

I. Introduction

A. Motivation

THE REMARKABLE escalation of the renewable energy-based distributed generation has created several challenges, among which islanding detection is the predominant one and widely debated over years. Failure in the detection of islanding event may create several power quality issues and stability problem. Over the years different techniques have been proposed to detect the islanding phenomenon. The existing commercial schemes such as remote control (RC), local control (LC), transform based, artificial intelligence (AI) and signal processing (SP) based techniques have certain drawbacks. The RC based techniques are expensive when it comes to the small networks whereas in LC based techniques it is difficult to define the threshold. Also, it suffers from large NDZ region, degraded power quality and high detection time. The computational time for transform based methods is very high. The AI algorithms are difficult to implement in practice and SP methods require high sampling frequency and gives poor response under noisy conditions. Therefore, the authors in this work seek to outline a comprehensive data-driven framework which is based on Lissajous figure obtained by plotting voltage waveforms versus current waveforms. The shape of the Lissajous figures can provide distinct insight about the type of disturbance in the power distribution network. The proposed technique exploits the characterizing patterns of the Lissajous figure to detect islanding phenomenon.

Manuscript received 19 January 2023; revised 29 April 2023 and 10 August 2023; accepted 3 October 2023. Date of publication 10 October 2023; date of current version 23 April 2024. Paper no. TSG-00082-2023. *(Corresponding author: Yadala Pavankumar.)*

The authors are with the Electrical Engineering Department, Jadavpur University, Kolkata 700032, India (e-mail: ypavankumar.ee.rs@jadavpuruniversity.in).

Color versions of one or more figures in this article are available at https://doi.org/10.1109/TSG.2023.3322435.

Digital Object Identifier 10.1109/TSG.2023.3322435

B. Literature Review

The depletion of the fossil fuels and growing concerns on environmental issues lead to the rapid enhancement in the penetration of renewable based distributed generation (DG) units into the distribution network. The integration of the DGs into the modern power systems brings several benefits such as high efficiency, reliability and improved power quality which have escalated the concept of smart microgrid. But the high integration of the DGs into the distribution network causes several security and protection issues, one of the important issues is islanding detection of the DGs. Failure to trip the islanded DG can cause severe problems and in the case of unintentional islanding, the DG must be disconnected within 2s as per the standards mentioned in IEEE 1547 standards [1]. Therefore, this issue gained rapid interest and the researchers presented various methods for islanding detection in the microgrid. The islanding detection techniques presented in the literature can be broadly categorized into two categories which are remote and local control techniques. In remote control approach the communication channel plays an important role to access the information from the remote terminals. The studies presented in [2], [3] monitored and analyzed the remote data constantly with the help of the supervisory control and data acquisition (SCADA). In [4] the authors presented a remote control method for islanding detection. These remote communication-based methods are not economical for the small network systems and these studies are not suitable where regional monitoring is required. Therefore, to overcome these issues the local control approaches are introduced. In the local control approaches the system parameters such as current, voltage and frequency are regionally monitored. These approaches are basically grouped into three categories, which are passive, active and hybrid methods. The passive approach basically depends on the variations of the system parameters such as rate of change of voltage phase angle [5], rate of change of kinetic energy over reactive power

(ROCOKORP) [6], sequence impedance [7], [8], phase angle difference of impedance [9] and adaptive rate of change of frequency [10]. The drawbacks of these passive methods are inability to detect islanding when power mismatch is low and at perfect power balance conditions. Moreover, these methods have large NDZ. Active islanding detection approaches gained more interest because of the shortcomings of passive islanding detection methods. Some of the active islanding detection studies presented in the literature are active ROCOF [11], reactive and active power control based method for synchronous machine type DGs [12], frequency deviation [13], phase disturbance [14] and sliding mode frequency shift [15]. The main problem of these active islanding methods is that due to the insertion of additional disturbance signal, the power quality of the system deteriorates. To avail the benefits of both active and passive methods, hybrid islanding detection methods are developed. One of such methods is presented in the literature which is based on the parallel inductance switching [16].

Later on the researchers developed S-transform and wavelet transform based islanding detection techniques [17], [18], [19]. The computational time for S-transform based methods is very high which is not suitable for practical applications and also it is not possible for S-transform to incorporate all signals inside the predetermined Gaussian window. Wavelet transform based methods have drawbacks such as hardware limitations and high sampling rate. Subsequently, Hilbert Huang transform based approaches have been proposed for islanding detection applying empirical mode decomposition [20], [21]. The authors in [22], [23] proposed islanding detection methods based on the pattern recognition and neuro fuzzy interface system. However, large number of neurons, complex training process and large training sets are the disadvantages of these approaches.

The authors in [24] developed an event index value based on the super imposed components of the sequence impedance by acquiring the local data. The authors in this work have not considered synchronous generator based DG. In [25] an islanding detection technique has been developed by injecting disturbance in the maximum power point control when the voltage exceeds the desired threshold. But it is only limited to the photovoltaic based systems whereas, in this work different types of DGs have been considered. A new islanding detection index is proposed in [26] based on the rate of change of potential energy function. In [27] the authors proposed a PMU based technique which has been developed considering the change in the phasors of the pre disturbance and post disturbance voltage and current signals.

In recent years the utilization of waveform measurement units (WMU) as a smart sensor has been introduced. The WMU can provide precise information of the time synchronized current and voltage waveform measurements and has high reporting rate. Lissajous figure can be developed utilizing the voltage and current waveforms [28]. The Lissajous figure reveals different behavior under different conditions which can be utilized to identify the cause of events in the system. Therefore, the authors in this work seek to propose a new islanding detection method for microgrid by utilizing the characteristics of the Lissajous figure.

C. Summary of Technical Contributions

This work presents a novel approach for islanding detection in the microgrid which consists of various types of DGs based on the Lissajous figure characteristics at each DG. The main contributions of this work can be summarized as follows:

1) A new approach for islanding detection in microgrid based on the change of shape of Lissajous curve has been proposed. The shape of the Lissajous curve which is an ellipse under normal condition changes when disturbance occurs. The distinct pattern in the change of shape during islanding condition has been captured to segregate the islanding event from other disturbances.
2) Adaptive thresholding based on Otsu algorithm has been considered for threshold selection to differentiate the non-islanding and islanding events.
3) The Lissajous figures provide insight into the state of operation of power system and the SI values can indicate the start time of the islanding event.
4) The proposed method can detect islanding for different types of DGs. The model considered in this paper includes photovoltaic, wind and synchronous generator.

II. Islanding Detection Using Lissajous Figure

The voltage and current signals collected from the PCC in the microgrid can be graphically represented in the form of a Lissajous curve.

A. Representation of Lissajous Figure

The instantaneous voltage and current signals can be represented as

$$v = V_m \ sin \ (wt) \tag{1}$$

$$i = I_m \ sin \ (wt + \theta) \tag{2}$$

where θ is the power factor angle and V_m and I_m are the amplitudes of the voltage and current signal respectively. The Lissajous figure is constructed with the current signal in the x-axis and the voltage signal in the y-axis. Eliminating the time variable wt from (1) and (2), formula correlating v and i can be obtained as follows

$$wt = sin^{-1}\left(\frac{i}{I_m}\right) - \theta = sin^{-1}\left(\frac{v}{V_m}\right) \tag{3}$$

Solving (3) using the trigonometric identities, (4) can be obtained.

$$\frac{i^2}{I_m^2} + \frac{v^2}{V_m^2}cos^2\theta - 2\frac{vi}{I_m V_m}cos\theta = sin^2\theta \tag{4}$$

The quadratic equation (4) can be written as shown in (5).

$$Ax^2 + Bxy + Cy^2 + D = 0 \tag{5}$$

where

$$A = 1/I_m^2, \ B = -2\frac{cos\theta}{I_m V_m}, \ C = 1/V_m^2, \ D = -sin^2\theta$$

$$\text{and } B^2 - 4AC = -\frac{4sin^2\theta}{I_m^2 V_m^2} \tag{6}$$

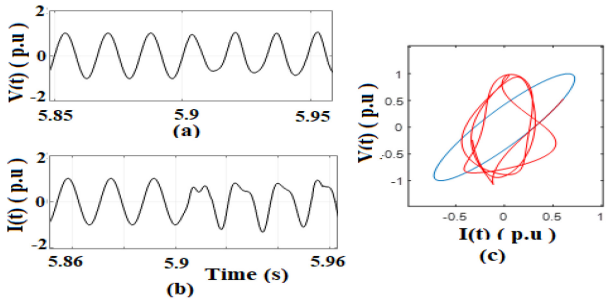

Fig. 1. Example of Lissajous figure: (a) Voltage signal, (b) Current signal, (c) Lissajous figure corresponding to voltage and current signal.

From (6) it can be observed that B^2-$4AC$ is a negative term regardless of the amplitude of I_m and V_m, and quadratic equation (4) represents an ellipse. Hence, mathematically it is evident that under normal conditions the Lissajous figure represents an ellipse. When islanding occurs, it creates disturbance in the voltage and current signals at the islanded circuit breaker which results the Lissajous figure to deviate from its original shape of an ellipse. Therefore, the shape of the Lissajous figure is different under islanding event. Fig. 1 depicts how Lissajous figure can been obtained from the voltage and current signals. Fig. 1(a) and Fig. 1(b) show the voltage and current signals and Fig. 1(c) shows the Lissajous figure obtained from the voltage and current signals. Under normal condition, the Lissajous curve is shown in blue color in Fig. 1(c) which represents an ellipse but when islanding occurs at 5.9s, the Lissajous curve deviates from the shape of an ellipse which is shown in red color. In this work, the distinct change in the pattern of Lissajous curve has been utilized to develop the islanding detection technique.

B. Islanding Detection

As mentioned in the above section, the Lissajous pattern varies under different conditions and accordingly the area of the Lissajous figure will also vary. Therefore, by determining the area of the Lissajous figure for successive intervals, a similarity index can be formulated to detect the disturbance event. The area of the Lissajous figure at time 't' can be calculated using (7).

$$A_{v-i}(t) = \left| \int_{i(\tau=t-T)}^{i(\tau=t)} v(\tau) di(\tau) \right| \tag{7}$$

Under normal condition the successive areas are almost same. For example, if $A_{v-i}(t)$ is the area at time 't' and $A_{v-i}(t-\Delta t)$ is the area at time '$t-\Delta t$', both will be almost same under normal operating condition where 'Δt' is the time interval. If any event occurs at time 't', there will be significant difference between the $A_{v-i}(t)$ and $A_{v-i}(t-\Delta t)$. Therefore, a similarity index has been formulated based on the area of the Lissajous figure as shown in (8) to detect the islanding condition.

$$SI(t) = 1 - \left| \frac{A_{v-i}(t) - A_{v-i}(t-\Delta t)}{max\{A_{v-i}(t), A_{v-i}(t-\Delta t)\}} \right| \tag{8}$$

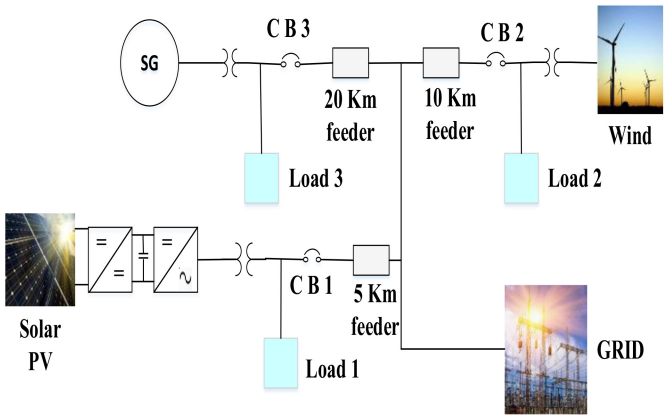

Fig. 2. Microgrid test system.

The value of SI will vary from 0 to 1. Under normal condition or before islanding the successive areas are almost equal and hence, the value of SI is near to 1 whereas, after islanding there is a significant difference between the successive areas which results in the value of SI to deviate from 1. Even after the islanding event it is observed that there is a significant change in the successive areas and the value of SI remains less than 1. Therefore, by choosing a proper threshold for SI, islanding condition has been detected in this study.

C. Implementation of the Proposed Algorithm

Based on the above analysis, an algorithm has been developed to detect islanding in the test system shown in Fig. 2. The test system consists of three different DGs which are connected to the system through the circuit breakers [6]. As different types of DGs are connected in the microgrid, it is possible that the behavior of each DG may vary due to change of events. Hence, to accurately detect the islanding in the proposed system, a threshold (SI_{th}) has been determined for the SI. The SI value at CB3 is considered initially followed by SI at other breakers to identify islanding condition. It is noteworthy to mention that the change in the area of Lissajous figure may occur not only due to islanding event but also due to the short circuit faults, load switching and other transient events. If SI at CB3 is less than SI_{th}, then islanding condition occurs at CB3. It is also possible that in this case there is multiple islanding involving DG at CB3. Next, the SI values will be checked at CB1 and CB2. SI values will remain less than SI_{th} for more than 5 cycles if the DGs at CB1 and CB2 are islanded. The detailed flowchart of the proposed algorithm is shown in Fig. 3.

Though the algorithm shown in the flowchart considers SI values at CB3 first, the algorithm can start considering CB1 or CB2 also. It is to be noted that during islanding the duration for which SI values remain below the threshold value in case of synchronous based DG, is less than other two DGs which has been discussed in the next section. The flowchart shown in Fig. 3 can be modified considering SI values at CB1 or CB2 at starting instead of CB3. Moreover, the developed algorithm is not network specific. It can be applied to other networks also.

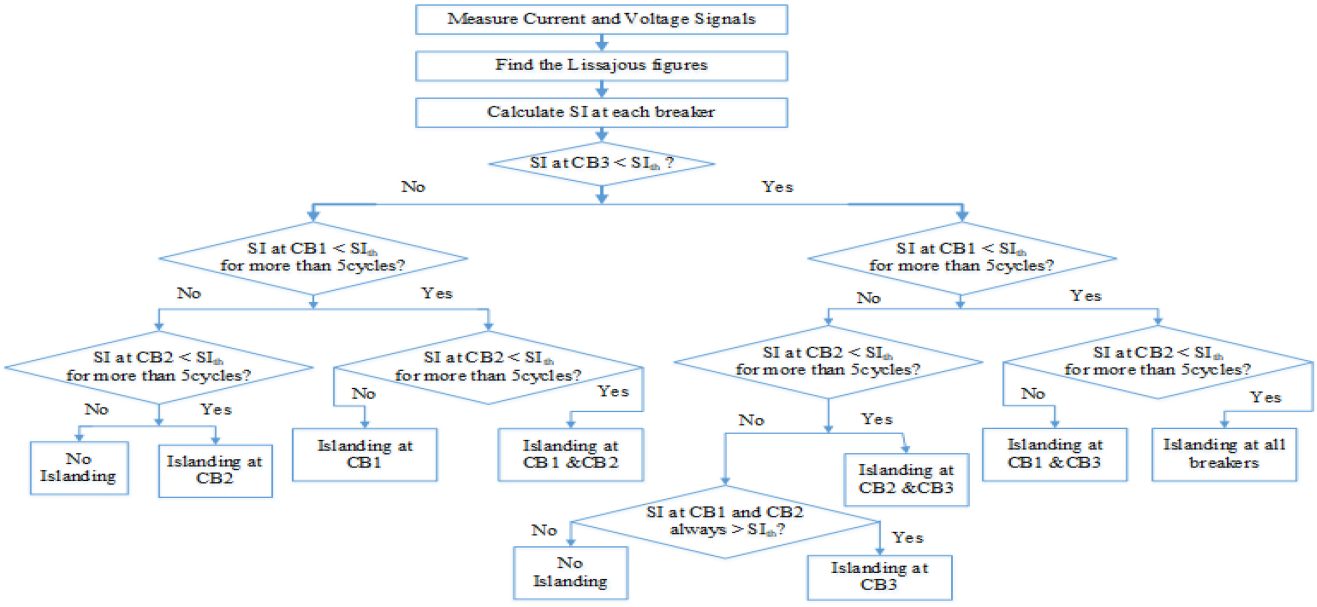

Fig. 3. Proposed islanding detection algorithm.

III. Simulation Results

The test system considered in this study as shown in Fig. 2 consists of three types of DGs which are photovoltaic, wind and synchronous generator based DGs with the rating of 250kW, 500kW and 200kW, respectively. Three different parallel RLC loads are connected to each DG. Load 1 consists of R_1=2.5 kΩ, L_1=4.421 H and C_1=1.59 μF, load 2 consists of R_2=1.25 kΩ, L_2=2.21 H and C_2=3.183 μF, load 3 consists of R_3=3.125 kΩ, L_3=5.53 H and C_3=1.237μF, respectively. The DG input voltage, reference temperature and voltage of photovoltaic DG are 500V, 45°C and 260V (ph-ph), respectively. Inertia constant, friction factor and output voltage for synchronous generator based DG are 3.2, 0 and 13.8kV, respectively and for wind based DG those are 0.685, 0.01 and 575V, respectively. The grid frequency is considered as 60Hz, operating voltage is 25 kV and the feeder lengths are shown in Fig. 2. The proposed islanding detection technique has been evaluated under different conditions as discussed in the following subsections. Under normal condition the *SI* remains above the threshold but under islanding condition it will be lower than the threshold value. It is possible that the shape of the Lissajous figure at non islanded breakers may alter due to other transient conditions resulting the *SI* values at the non-islanded CBs to come down below the SI_{th}. Therefore, to accurately detect the islanding condition another additional criterion is considered in the decision making. If *SI* remains less than SI_{th} for more than 5 consecutive samples at CB1 and CB2, then islanding event is detected. To detect islanding the proposed algorithm requires at least 5 consecutive cycles data and the maximum computational time to execute the algorithm is 0.1179s.

A. Threshold Selection

It is important for an islanding detection method to distinguish islanding from other disturbance events such as short circuit faults, load switching, capacitor bank switching, etc. Therefore, the threshold selection plays an important role to properly distinguish the islanding from other disturbance events. To achieve this, in this study, Otsu algorithm based thresholding method has been used to select a robust threshold, which is reliable and has been widely used in threshold based techniques [20]. Initially the *SI* values for islanding scenarios and the non-islanding scenarios have been separated as class 1 and class 2 respectively. The probability density function (PDF) is assigned for both the classes in which the probability of different ranges of *SI* value is predicted based on the measured data. Then histogram has been plotted to obtain the probability of predicted *SI* for both the classes A comparative assessment has been carried out considering Weibull, Gama, and lognormal PDFs as shown in Table I. Weibull PDF is used to characterize the behaviour of the class 1 and class 2 events as it provided good fit (less K-S error, and high R^2 value) for the obtained histogram of the different scenarios in this study compared to Gamma and lognormal PDFs. The fitted PDF curves are intersecting at some point which is considered as the threshold to differentiate the class 1 and class 2 events.

TABLE I
Statistical Errors for Different Distribution Functions

PDF	K-S error	R^2
Weibull	0.2704	0.8297
Gama	0.2728	0.7925
Lognormal	0.2781	0.7314

Fig. 4. represents the PDF based Otsu thresholding analysis at CB1. It can be seen from Fig. 4 that the islanding and non-islanding PDF curves are intersecting at 0.9. Hence, the threshold for PV (CB1) is considered as 0.9. The same analysis is carried out for other DGs and the same value of threshold has been obtained for other DGs as well.

B. Evaluation of Islanding Detection Algorithm

In this case study the results are presented for different islanding conditions, such as CB of only one DG is opened and other CBs are closed (single islanding) or the CBs of

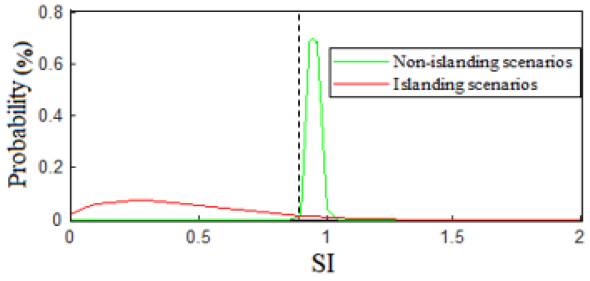

Fig. 4. Otsu thresholding analysis for PV.

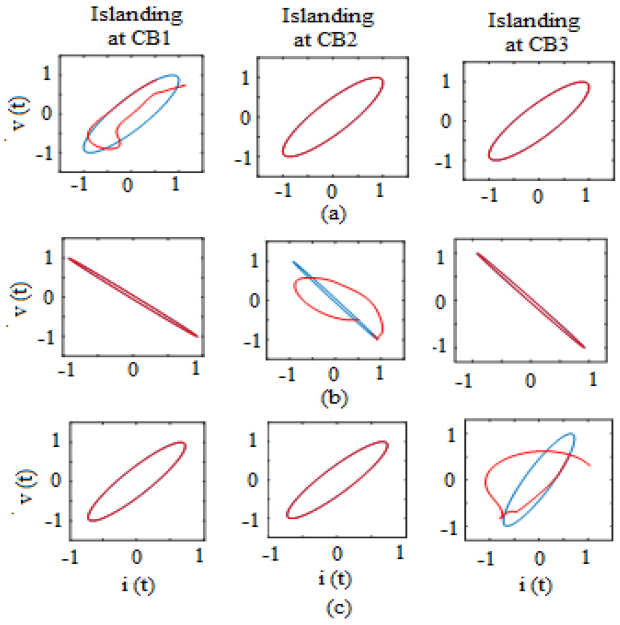

Fig. 5. Lissajous figures when islanding occurs at different DGs: (a) Lissajous figure at CB1, (b) Lissajous figure at CB2, (c) Lissajous figure at CB3.

multiple DGs are opened simultaneously (multiple islandings). The islanding condition is considered to occur at 5.9s and the voltage and current signals at each breaker have been used get the Lissajous figure as shown in Fig. 5. The blue color line indicates Lissajous curve before islanding and the red color line indicates after islanding. It can be seen from Fig. 5 that when islanding occurs at CB1, only the shape of the Lissajous figure at CB1 is altered (red color) whereas the shape of the Lissajous figures at other breakers remain same as before. The area of the Lissajous figure is calculated for each cycle and *SI* is calculated using (8) and presented in Fig. 6

From Fig. 6(a) it is observed that under normal condition (till 5.9s) the *SI* values at each breaker are above the threshold value but when islanding occurs at CB1 only, the value of *SI* at CB1 is less than the threshold for more than 5 consecutive samples after 5.9s and the value of *SI* at other breakers are above the threshold value. Similarly, when wind based DG is islanded, the value of *SI* at CB2 only is less than the threshold for more than 5 continuous samples after 5.9s as shown in Fig. 6(b). When islanding at CB3 occurs, the value of *SI* at CB3 is below the threshold and at other breakers it is above the threshold as shown in Fig. 6 (c). Therefore, the *SI* value detects islanding at 5.9s in all the three cases.

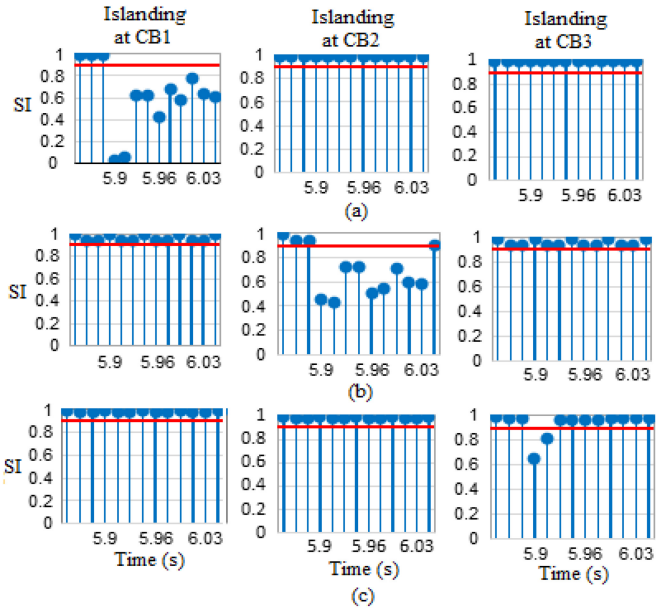

Fig. 6. *SI* values when islanding occurs at different DGs: (a) *SI* at CB1, (b) *SI* at CB2, (c) *SI* at CB3.

The proposed algorithm is evaluated when multiple breakers are opened simultaneously. Lissajous figures are obtained at different combinations of multiple islandings and it is observed that the shape of the Lissajous figures after islanding are deviating significantly only at the islanded CBs. In Table II, the *SI* values at each breaker are shown when the DGs connected to CB1 and CB2 are islanded simultaneously at 5.9s. It is visible that the value of *SI* at CB1 and CB2 is below the threshold value for more than 5 consecutive samples and it is not below the threshold value at CB3. Similarly, when all the CBs opened simultaneously, the values of *SI* at CB1 and CB2 are below the threshold value for more than 5 consecutive samples and also it is less than the threshold value at CB3 after 5.9s. Therefore, islanding at all the breakers is detected. It is to be noted that to detect islanding event at CB1 and CB2, the voltage and current signals collected only from the respective terminals are required. Islanding at the particular CB can be identified if the *SI* value is less than threshold for more than 5 consecutive cycles. But, to distinguish islanding event from other transient events at CB3, it requires the information of *SI* from other two breakers also. Hence, any communication delay in the data transfer may lead to the delay in the islanding event detection at CB3.

C. Evaluation Under NDZ Region

The proposed algorithm has been tested under the NDZ region of the frequency and voltage relays. Various loads have been considered inside of the NDZ region of voltage (0.88 to 1.1 p.u) and frequency (59.3 to 60Hz) with different active power imbalance (ΔP). The selection of the loads is done to assure that the reactive power imbalance is zero which makes the islanding detection difficult for the conventional relays. The performance of the algorithm has been analyzed under two cases as given in Table II. The active power imbalance is considered with zero reactive power imbalance. In the first

TABLE II
THE OUTPUT RESULTS OF THE PROPOSED TECHNIQUE FOR ISLANDING DETECTION

Condition			No. of Consecutive Samples of SI less than the Threshold		
			At CB1	At CB2	At CB3
Islanding		CB1	10	0	0
		CB2	0	12	0
		CB3	0	0	2
		CB1 & CB2	10	12	0
		CB2 & CB3	0	11	2
		CB3 & CB1	10	0	2
		All	10	12	2
UL1741	Case 1	CB1	10	0	0
		CB2	0	12	0
		CB3	0	0	2
	Case 2	CB1	12	0	0
		CB2	0	14	0
		CB3	0	0	2
	Case 3	CB1	12	0	0
		CB2	0	12	0
		CB3	0	0	2
	Case 4	CB1	13	0	0
		CB2	0	14	0
		CB3	0	0	2
	Case 5	CB1	13	0	0
		CB2	0	14	0
		CB3	0	0	2
NDZ	ΔP= -5kW	CB1	11	0	0
		CB2	0	13	0
		CB3	0	0	2
	ΔP= 10kW	CB1	10	0	0
		CB2	0	14	0
		CB3	0	0	2
Load quality factor	Q_f=1	CB1	12	0	0
		CB2	0	13	0
		CB3	0	0	2
	Q_f=2.5	CB1	13	0	0
		CB2	0	15	0
		CB3	0	0	3

case the active power imbalance is considered as −5kW and when islanding occurs at CB2 at 5.9s, it can be seen from Table II that the value of the *SI* is less than the threshold for more than 5 consecutive samples at CB2. In the second case, the active power imbalance is considered as 10 kW, the *SI* values for different islandings are tabulated in Table II. In all the cases the proposed algorithm is able to identify the islanding event.

D. UL1741 Test Conditions

The reliability of the proposed method is verified under the test conditions of UL1741 for islanding protection of the DGs. As per the UL1741 test conditions, the load active power of the DG is adjusted to 100%, 50% and 25% and also the reactive power is adjusted between −5% to 5%. Based on these conditions five scenarios of simulation studies are conducted on the test system shown in Fig. 2 to evaluate the proposed method.

Case 1: The active power and reactive power consumption of the load is 100% and 0%, respectively (unity pf).

Case 2: The active power and reactive power consumption of the load is 50% and 0%, respectively (unity pf).

Case 3: The active power and reactive power consumption of the load is 25% and 0%, respectively (unity pf).

Case 4: The active power and reactive power consumption of the load is 100% and -1%, respectively (leading pf).

Case 5: The active power and reactive power consumption of the load is 50% and 1%, respectively (lagging pf).

To establish the above mentioned scenarios different sets of RLC loads are considered at each DG. For each scenario the simulation studies are conducted for all the three DG islandings and the performance of the proposed method is tested. In Table II the obtained results of *SI* when islanding occurs at all the breakers under different cases are presented. The obtained results show that the performance of the proposed method is satisfactory under UL1741 test conditions.

E. Effect of Load Quality Factor

The behaviour of the proposed algorithm under different Quality factors (Q_f) has been verified in this case study. The standards emphasize that the most critical value of Q_f is 2.5 and it varies from 1 to 2.5. The higher Q_f creates problems in islanding detection. Assuming parallel RLC load, the values of R, L and C are computed as shown in (9) to (11).

$$R = \frac{V_r^2}{P_r} \tag{9}$$

$$L = \frac{V_r^2}{2\pi f_r P_r Q_f} \tag{10}$$

$$C = \frac{P_r Q_f}{2\pi f_r V_r^2} \tag{11}$$

where, V_r is the rated grid voltage, f_r is the resonant frequency, P_r is the rated power and Q_f is the quality factor. The performance of the proposed method is tabulated in Table II. All the CBs are opened at 5.9s. The test results are presented for all the three islandings for Q_f =1 and Q_f=2.5. It can be seen from the results that the islanding is detected accurately in all the cases.

F. Effect of Load Switching

The test model under this study is monitored while switching different linear and non-linear loads. In this section starting of 160 kVA induction motor and switching of 0.4 MVar capacitor bank are considered as tabulated in Table III. The results of the change of *SI* values when induction motor is started at PV based DG bus and capacitor bank switching at CB2 at 5.9s are tabulated in Table IV. From Table IV it can be seen that the values of *SI* are not below the threshold for more than 5 consecutive samples and hence the proposed method does not detect switching events as islanding.

G. Effect of Faults

In this section the effect of different types of faults on the performance of the proposed method is discussed. In this

TABLE III
SWITCHING AND FAULTS

Type	Value
Starting of induction motor	0-160 kVA
Capacitor bank switching	0-0.4 MVar
Faults (LG, LL, LLG, LLL, LLLG)	0-10Ω

TABLE IV
THE OUTPUT RESULTS OF THE PROPOSED TECHNIQUE UNDER NON-ISLANDING CONDITIONS

Type		No. of Consecutive Samples of SI less than the Threshold		
		At CB1	At CB2	At CB3
LG	Near CB1	3	2	1
	Near CB2	2	4	1
	Near CB3	1	1	2
LL	Near CB1	3	2	1
	Near CB2	1	4	1
	Near CB3	1	2	2
LLG	Near CB1	4	4	4
	Near CB2	1	4	1
	Near CB3	1	2	2
LLL	Near CB1	3	3	1
	Near CB2	2	3	1
	Near CB3	2	2	3
LLLG	Near CB1	4	3	1
	Near CB2	2	4	1
	Near CB3	2	2	4
Starting of Induction Motor	Near CB1	0	0	0
	Near CB2	0	0	0
	Near CB3	0	0	0
Capacitor Switching	Near CB1	2	1	0
	Near CB2	0	2	0
	Near CB3	0	3	3

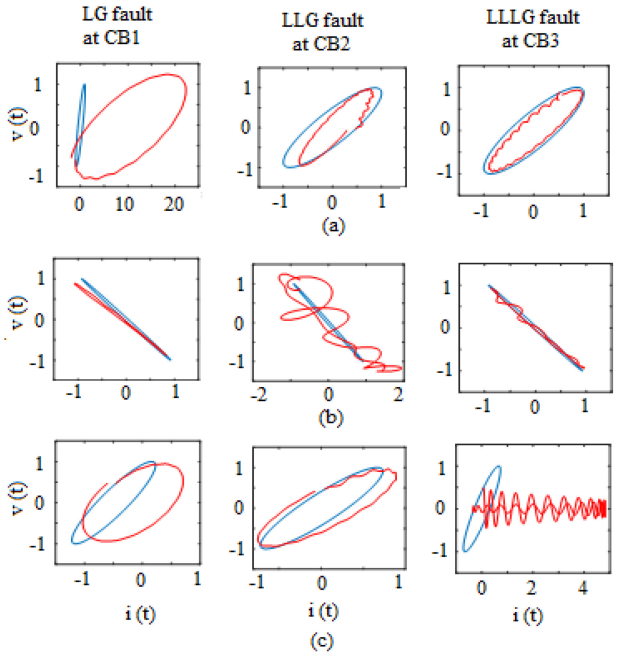

Fig. 7. Lissajous figure under faults: (a) Lissajous figure at CB1, (b) Lissajous figure at CB2: (c) Lissajous figure at CB3.

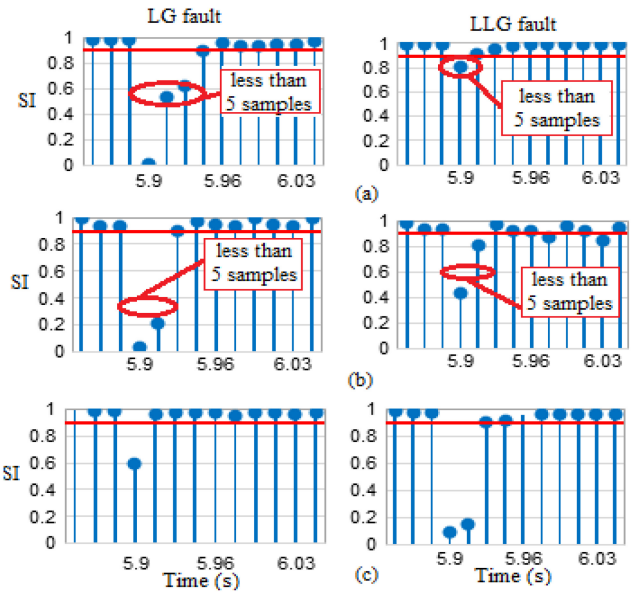

Fig. 8. Behaviour of *SI* under different types of faults: (a) *SI* at CB1, (b) *SI* at CB2, (c) *SI* at CB3.

case different fault types with different fault resistances are considered and the fault has been applied at each feeder at 5.9s. The Lissajous figures for some selected cases are presented in Fig. 7. When fault occurs at any location, it is observed that all the DG terminals experience disturbance in voltage and current signals which results in the abrupt change in the shape of the Lissajous figure at every breaker. But the shape of the Lissajous figure at each breaker regain its original shape within 5 cycles. The *SI* values have been calculated and presented in Fig. 8 and Table IV. From Fig. 8 it can be observed that when fault occurs there is a change in the value of *SI* at all breakers but the value of *SI* is not below the threshold for more than 5 consecutive samples. Therefore, it is not satisfying the criteria of islanding according to the proposed method and hence it is not detected as islanding event.

H. Effect of Sensing Errors

The proposed approach has been tested in the presence of sensing errors in the measured voltage and current signals within the range of ±3 % following IEEE/ANSI standards [29]. Two cases are considered to evaluate the proposed approach. In case 1 it is considered that the signals measured from CB3 are having sensing errors from 5.9s under normal condition. From Fig. 9(a) it can be seen that there is a slight change in the shape of the Lissajous curve at CB3 due to presence of sensing errors (in red color). Then *SI* has been computed at CB3 as shown in Fig. 9(b). Fig. 9(b) reveals that

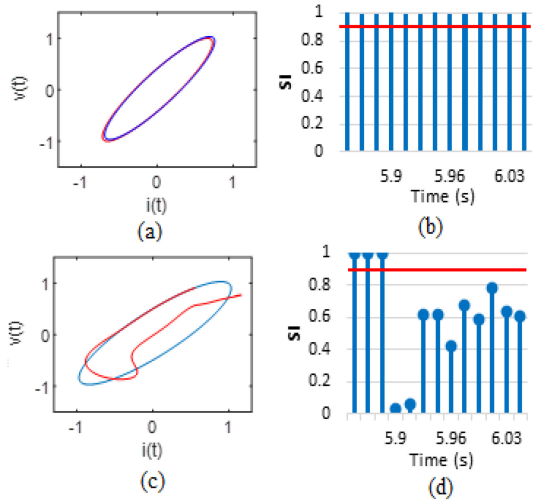

Fig. 9. Performance of the proposed approach under sensing errors: (a) Lissajous curve at CB3 in Case 1, (b) Behavior of *SI* at CB3 in Case 1, (c) Lissajous curve at CB1 in Case 2, (d).

there is not much change in the behavior of the *SI* at CB3. In Case 2 it is considered that the sensing errors are present in the measured signals from the beginning and islanding event occurs at CB1. The Lissajous curve corresponding to the signals at CB1 is shown in Fig. 9(c) and the behavior of *SI* at CB1 is depicted in Fig. 9(d). The results indicate that the performance of the proposed approach has not deteriorated due to the sensing errors.

I. Hardware- in-the-Loop Testing

In recent times the hardware in loop testing (HIL) has become the alternative to traditional simulation testing for validating proposed technique before deployment which is being widely as used industry standard around the world. The HIL simulation creates the similar dynamics of the real hardware with the real time simulator; indirectly it produces the virtual plant which duplicates the real hardware. Therefore, using the HIL testing the proposed method has been validated for the real time applications in this study. The HIL testing setup considered in this study consists of four parts which are i) RT Lab software which is used to run the simulation in real time digital simulator, ii) Real time digital simulator (RTDS) which is the industrial standard HIL testing equipment; RTDS simulates the proposed system in real time. iii) Multi-channel digital oscilloscope which acts as the external waveform measurement unit (WMU) hardware to store and save the waveform data, iv) Computer unit which runs the RT lab, stores the measurement data and executes the algorithm.

The test model considered in Fig. 2 has been simulated in RTDS through the RT lab software for case (iv) of UL1741 when islanding occurs at CB1 to check the suitability of the proposed technique in real time applications. The voltage and current signals are collected from the digital oscilloscope at every circuit breaker to develop the Lissjous figures and the similarity index has been computed. The measured voltage and current signals at CB1 are shown in Fig. 10 (a) and 10 (b). The Lissajous figure and *SI* at CB1 are shown in Fig. 10 (c) and 10 (d), respectively. It can be seen from Fig. 10, that the islanding

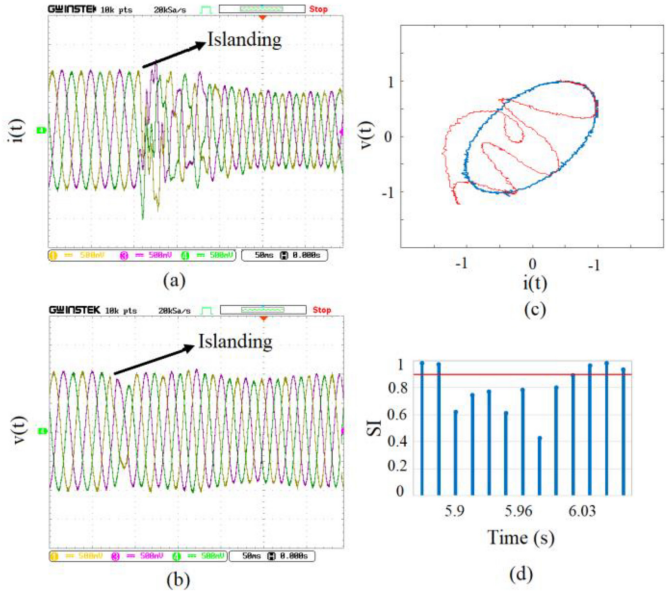

Fig. 10. HIL testing results of islanding at CB1 under UL1741: (a) Measured current signal, (b) Measured voltage signal, (c) Lissajous figure, (d) Similarity index.

occurs at 5.9s and *SI* value is less than the threshold for more than 5 consecutive cycles which is not true for other CBs. Therefore, the proposed algorithm detects the islanding at CB1 only.

IV. Comparative Assessment

The performance of the proposed method has been compared with the recent islanding detection methods based on the specifications as summarized in Table III. The methods reported in [14], [21], [22] can be operated only in the presence of the specified DG type. The ability of handling different types of DGs at different locations has not been considered. The proposed analysis considered various types of DGs widely used and is able to detect multi-islanding situations also. The islanding detection under NDZ region of voltage and frequency is sensible under small and zero power imbalances. Unlike the studies presented in [9], [14], different active power and reactive power unbalance have been considered in the proposed method which makes it robust against the NDZ. Different case studies under the test conditions of UL1741 for the protection of islanding DGs have been conducted in this work and accuracy of the islanding detection of the proposed method under UL1741 conditions is high unlike methods proposed in [21], [22]. The robustness of the proposed method has been validated for several non-islanding conditions which are having similar dynamics as that of islanding such as short circuit faults, capacitor switching and induction motor starting, etc. Unlike [9], [21], [22], the proposed method can distinguish other similar conditions which produce similar transients as that of islanding. The proposed method uses voltage and current signals at PCC only to detect islanding and synchronization of signals at different location is not necessary unlike [9]. The proposed method does not depend on the model architecture and complexity. Therefore, the proposed method is accurate and has less computational burden. Moreover, unlike

TABLE V
COMPARATIVE ASSESSMENT

Method	Type of DG	Faults	Q_f	Capacitor Switching	IMS	NDZ	UL1741	AI (%)	RTV
Ref [9]	PV	√	√	√	×	×	×	-	√
Ref [21]	SG	×	×	√	×	√	×	68.6	×
Ref [6]	PV, SG &WT	√	√	√	√	√	√	99	√
Ref [5]	Inverter based DG	√	√	×	×	√	√	-	×
Ref [22]	PV	√	√	×	×	√	√	78	√
Ref [14]	Inverter based DG	×	×	×	×	×	×	-	×
Proposed Method	PV, SG & WT	√	√	√	√	√	√	99	√
IMS- Induction motor starting, AI- Accuracy of islanding, RTV- Real time validation									

the methods proposed in [5], [14], [21] the proposed method has been validated using HIL testing for real time applications.

V. DISCUSSIONS

In the previous sections the performance of the proposed Lissajous based technique has been assessed under diverse islanding conditions such as NDZ, UL1741, variation in load quality factor, etc. Also, various case studies which may confuse islanding event with other events such as load changes, short circuit faults, induction motor starting and capacitor bank switching have been performed to test the efficacy of the proposed method. The proposed scheme does not require synchronized measurement of voltage and current signals and hence, it does not require expensive communication devices and free from synchronization error. Moreover, the proposed technique does not have any adverse effect on the power quality of the microgrid unlike active islanding detection techniques. It is not dependent on the DG penetration level and suitable for islanding detection of all types of commonly used DGs. The proposed technique involves low computational complexity compared to other transform based and AI based schemes. As it involves simple mathematical calculations and requires less memory space, this algorithm can be easily programmed and implemented in numerical relays. A relay compatible sampling frequency of 10 kHz along with fast rate of islanding detection makes this islanding detection technique suitable for implementation in real microgrid.

However, it has been observed that the proposed algorithm fails to detect islanding condition for the worst load quality factor of 4 [9]. Also, the algorithm of islanding detection for synchronous generator is different from other DGs. Islanding detection for synchronous generator requires the information of the status of other DG terminals and hence, any miscommunication may generate false alarm for islanding detection of synchronous generator.

Smart grids nowadays have become prone to cyber-attacks which adversely affect its security and reliability. To ensure cyber-security, bad data detection and elimination is essential which has not been incorporated in this paper. This work can be extended to islanding detection considering cyber-security.

VI. CONCLUSION

This work presents a novel technique to detect islanding in microgrid by utilizing the Lissajous figure patterns. A similarity index has been developed based on the characteristics of the Lissajous figure at each circuit breaker of the DG to identify the islanding condition and distinguish it from other similar conditions. Otsu algorithm based adaptive thresholding is considered in this study to select the threshold and the proposed algorithm utilizes only the voltage and current signals at the particular DG. The simulation results show that the proposed method is able to detect the islanding even in the presence of different DG types. The proposed algorithm is tested under diverse conditions and the performance of the proposed algorithm is satisfactory. Moreover, the proposed method is validated on HIL testing for real time applications and the comparative study shows that the proposed method has high accuracy.

REFERENCES

[1] *IEEE Standard for Interconnection and Interoperability of Distributed Energy Resources with Associated Electric Power Systems Interfaces*, IEEE Standard 1547, 2018.

[2] M. A. Redfern, O. Usta, and G. Fielding, "Protection against loss of utility grid supply for a dispersed stoarage and generation unit," *IEEE Trans. Power Del.*, vol. 8, no. 3, pp. 948–954, Jul. 1993.

[3] A. M. Massoud, K. H. Ahmed, S. J. Finney, and B. W. Williams, "Harmonic distortion-based island detection technique for inverter-based distributed generation," *IET Renew. Power Gener.*, vol. 3, no. 4, pp. 493–507, 2009.

[4] W. Xu, G. Zhang, C. Li, W. Wang, G. Wang, and J. Kliber, "A power line signaling based technique for anti-islanding protection of distributed generators—Part I: Scheme and analysis," *IEEE Trans. Power Del.*, vol. 22, no. 3, pp. 1758–1766, Jul. 2007.

[5] H. Samet, F. Hashemi, and T. Ghanbari, "Islanding detection method for inverter-based distributed generation with negligible non-detection zone using energy of rate of change of voltage phase angle," *IET Gener. Transm. Distrib.*, vol. 9, no. 15, pp. 2337–2350, 2015.

[6] H. Khosravi, H. Samet, and M. Tajdinian, "Robust islanding detection in microgrids employing rate of change of kinetic energy over reactive power," *IEEE Trans. Smart Grid*, vol. 13, no. 1, pp. 505–515, Jan. 2022.

[7] P. Kumar, V. Kumar, and B. Tyagi, "Islanding detection for reconfigurable microgrid with RES," *IET Gener. Transm. Distrib.*, vol. 15, no. 7, pp. 1187–1202, 2021.

[8] H. Muda and P. Jena, "Rate of change of superimposed negative sequence impedance based islanding detection technique for distributed generations," *IET Gener. Transm. Distrib.*, vol. 10, no. 13, pp. 3170–3182, 2016.

[9] R. Nale, M. Biswal, and N. Kishor, "A passive communication based islanding detection technique for AC microgrid," *Int. J. Electr. Power Energy Syst.*, vol. 137, May 2022, Art. no. 107657.

[10] M. W. Altaf, M. T. Arif, S. Saha, S. N. Islam, M. E. Haque, and A. M. T. Oo, "Effective ROCOF based islanding detection technique for different types of microgrid," in *Proc. IEEE Ind. Appl. Soc. Annu. Meeting (IAS)*, 2021, pp. 1–8.

[11] P. Gupta, R. S. Bhatia, and D. K. Jain, "Active ROCOF relay for islanding detection," *IEEE Trans. Power Del.*, vol. 32, no. 1, pp. 420–429, Feb. 2017.

[12] R. Zamani, M. E. Hamedani-Golshan, H. H. Alhelou, P. Siano, and H. R. Pota, "Islanding detection of synchronous distributed generator based on the active and reactive power control loops," *Energies*, vol. 11, no. 10, p. 2819, 2018.

[13] P. Gupta, R. S. Bhatia, and D. K. Jain, "Average absolute frequency deviation value based active islanding detection technique," *IEEE Trans. Smart Grid*, vol. 6, no. 1, pp. 26–35, Jan. 2015.

[14] T. Z. Bei, "Accurate active islanding detection method for grid-tied inverters in distributed generation," *IET Renew. Power Gener.*, vol. 11, no. 13, pp. 1633–1639, 2017.

[15] D. Voglitsis, F. Valsamas, N. Rigogiannis, and N. Papanikolaou, "On the injection of sub/inter-harmonic current components for active anti-islanding purposes," *Energies*, vol. 11, no. 9, p. 2183, 2018.

[16] A. Rostami, A. Jalilian, S. Zabihi, J. Olamaei, and E. Pouresmaeil, "Islanding detection of distributed generation based on parallel inductive impedance switching," *IEEE Syst. J.*, vol. 14, no. 1, pp. 813–823, Mar. 2020.

[17] P. K. Ray, N. Kishor, and S. R. Mohanty, "Islanding and power quality disturbance detection in grid-connected hybrid power system using wavelet and S-transform," *IEEE Trans. Smart Grid*, vol. 3, no. 3, pp. 1082–1094, Sep. 2012.

[18] A. Samui and S. R. Samantaray, "Wavelet singular entropy-based islanding detection in distributed generation," *IEEE Trans. Power Del.*, vol. 28, no. 1, pp. 411–418, Jan. 2013.

[19] S. Alshareef, S. Talwar, and W. G. Morsi, "A new approach based on wavelet design and machine learning for islanding detection of distributed generation," *IEEE Trans. Smart Grid*, vol. 5, no. 4, pp. 1575–1583, Jul. 2014.

[20] H. Khosravi, H. Samet, and M. Tajdinian, "Empirical mode decomposition based algorithm for islanding detection in micro-grids," *Electr. Power Syst. Res.*, vol. 201, Dec. 2022, Art. no. 107542.

[21] B. K. Chaitanya and A. Yadav, "Hilbert-Huang transform based islanding detection scheme for distributed generation," in *Proc. 8th IEEE Power India Int. Conf. (PIICON)*, 2018, pp. 1–5.

[22] D. Mlakic, H. R. Baghaee, and S. Nikolovski, "A novel ANFIS-based islanding detection for inverter-interfaced microgrids," *IEEE Trans. Smart Grid*, vol. 10, no. 4, pp. 4411–4424, 2019.

[23] S. R. Samantaray, B. C. Babu, and P. K. Dash, "Probabilistic neural network based islanding detection in distributed generation," *Electr. Power Compon. Syst.*, vol. 39, no. 3, pp. 191–203, 2011.

[24] P. Kumar, V. Kumar, and B. Tyagi, "A novel islanding detection technique based on event index value for reconfigurable microgrid," *IEEE Trans. Ind. Appl.*, vol. 57, no. 4, pp. 3451–3462, Jul./Aug. 2021.

[25] R. Bakhshi-Jafarabadi, J. Sadeh, and M. Popov, "Maximum power point tracking injection method for islanding detection of grid-connected photovoltaic systems in microgrid," *IEEE Trans. Power Del.*, vol. 36, no. 1, pp. 168–179, Feb. 2021.

[26] M. Tajdinian, H. Khosravi, H. Samet, and Z. M. Ali, "Islanding detection scheme using potential energy function based criterion," *Electr. Power Syst. Res.*, vol. 209, Aug. 2022, Art. no. 108047.

[27] Z. S. Chafi, H. Afrakhte, and A. Borghetti, "μPMU-based islanding detection method in power distribution systems," *Int. J. Electr. Power Energy Syst.*, vol. 151, Sep. 2022, Art. no. 109102.

[28] B. Patel, "A new technique for detection and classification of faults during power swing," *Electr. Power Syst. Res.*, vol. 175, Oct. 2019, Art. no. 105920.

[29] T. S. Abdelgayed, W. G. Morsi, and T. S. Sidhu, "A new approach for fault classification in microgrids using optimal wavelet functions matching pursuit," *IEEE Trans. Smart Grid*, vol. 9, no. 5, pp. 4838–4846, Sep. 2018.